JOURNAL OF MASS SPECTROMETRY, VOL. 33, 305–318 (1998)

A Quadrupole Ion Trap/Time-of-flight Mass Spectrometer with a Parabolic Reflectron

Vladimir M. Doroshenko and Robert J. Cotter*
Middle Atlantic Mass Spectrometry Laboratory, Department of Pharmacology and Molecular Sciences, The Johns Hopkins University School of Medicine, 725 N. Wolfe Street, Baltimore, Maryland 21205, USA

A matrix-assisted laser desorption/ionization-quadrupole ion trap/reflectron time-of-flight (MALDI-QIT/reTOF) mass spectrometer design and its operation in both normal and tandem mass spectrometric modes are described. A parabolic reflectron was found to be capable of providing mass resolution of 5000 for an initial ion energy distribution ranging over a 50% energy interval of the entire reflectron energy range. The sensitivity, ion isolation and fragmentation efficiency in the MALDI-QIT/reTOF instrument were close to those observed in the MALDI/QIT mass spectrometer. The mass resolution was shown to depend on the extraction field potentials, the r.f. trapping voltage amplitude and the phase of shutting down the r.f. voltage before extraction. At values of $q_z < 0.3$–0.4 the mass resolution does not depend on the ion mass, is in a range of 1000–1400 and is governed by the extraction voltages and the ion temperature before extraction, the latter shown to be in the range 1180–1690 K. The variation of the mass resolution for ions at values of $q_z > 0.4$ is irregular but normally it is lower than that for ions having lower q_z values. Mass spectral line positions shifted when the trapping voltage before extraction was varied. The line shifts were larger for lower mass ions and were comparable to the line widths in the case of very low masses.

J. Mass Spectrom. **33**, 305–318 (1998)

KEYWORDS: quadrupole ion trap; time-of-flight mass spectrometry; reflectron; mass resolution

INTRODUCTION

Although significant progress has been made in the development of quadrupole ion trap (QIT) mass spectrometers,[1] in some cases such as gas and liquid chromatography/mass spectrometry (GC/MS and LC/MS) or for studying ion–molecule reactions, the r.f. voltage amplitude scanning technique[2] commonly used for sequential ejection, detection and subsequent mass analysis lowers the duty cycle of the instrument and can severely limit the applications of the technology. One alternative approach is the development of a QIT/time-of-flight (TOF) mass spectrometer.[3]

The ejection of ions from a QIT for subsequent mass analysis in a quadrupole mass filter or a TOF mass spectrometer is an approach which has existed for many years[4–8] and was the main method of mass analyzing and studying the properties of the ion environment inside the QIT before the invention of the mass-selective axial instability mode of operation.[2] The idea of revisiting the QIT/TOF-MS instrumental combination has been inspired primarily by problems associated with interfacing an electrospray ionization (ESI) source (which produces ions continuously) with a TOF mass spectrometer (which operates in a pulsed mode).[9] In one sense, the coupling of continuous ionization with TOF analyzers was solved in 1955 by Wiley and McLaren[10] using delayed, pulsed extraction, but resulted in very low duty cycles. In a more recent method developed for interfacing continuous electrospray ionization (ESI) sources with TOF-MS, known as orthogonal extraction,[11–13] ions produced by ESI are extracted in a direction perpendicular to their initial velocity distribution. This provides some ion storage capability for increasing the duty cycle which nevertheless remains low. In an alternative approach, ions from an ESI source are introduced and accumulated in an ion trap and then injected into a TOF mass spectrometer for mass analysis.[3,14] In this case, the efficient ion storage capabilities of the ion trap, coupled with the short mass analysis times of the TOF stage, results in duty cycles that approach 100%. Thus, such instruments have proved useful for the detection and mass analysis of ions from low-intensity, continuous ion sources such as ESI[15] and atmospheric pressure ionization.[16]

Quadrupole ion traps,[14–16] cylindrical ion traps[17] and segmented ring traps[18] have all been interfaced to a TOF mass spectrometer. In this work we focused only on the three-dimensional hyperbolic traps which approach an ideal quadrupolar trapping field, since it is only in that case that high-resolution ion isolation, which is vital for tandem (MS/MS) experiments, can be achieved using resonance excitation techniques including broadband excitation.[19,20] In these traps, positive ions may be extracted by applying either a positive (repulsive) or negative (attractive) voltage pulse on the end-cap electrode furthest from and nearest to the TOF

* *Correspondence to*: R. J. Cotter, Middle Atlantic Mass Spectrometry Laboratory, Department of Pharmacology and Molecular Sciences, The Johns Hopkins University School of Medicine, 725 N. Wolfe Street, Baltimore, Maryland 21205, USA
E-mail: rcotter@welchlink.welch.jhu.edu
Contract grant sponsor: National Institute of Health; *Contract grant number*: R01 RR08912.

CCC 1076–5174/98/040305–14 $17.50

Received 10 March 1997
Accepted 12 December 1997

mass analyzer, respectively. In this case the r.f. voltage is usually removed from the ring electrode before ion extraction and the ring electrode is normally grounded during ion extraction. In early experiments,[21] attractive voltage pulses applied to the near end-cap electrode were shown to yield larger ion currents, and this approach has therefore been used in most of the recent efforts to interface quadrupole ion traps with TOF mass analyzers.[3,14–16,22,23] In another approach, symmetric repulsive/attractive voltage pulses are applied to the end-cap electrodes,[24,25] resulting in considerably better ion beam quality. This is explained by the removal of the sextupolar component of the electric field in this case, leaving the octopole component as the most significant higher order multipole.[26]

Given the fact that QIT/TOF configurations were developed primarily to support continuous ionization methods on a TOF mass analyzer, it might appear that the QIT/TOF combination provides no particular advantages over a QIT mass spectrometer, when the matrix-assisted laser desorption/ionization (MALDI) method is used as an ion source. However, the MALDI-QIT/TOF configuration provides new possibilities for studying processes related to MALDI and the trapping of ions.[23,27,28] The unique features of the MALDI-QIT/TOF instrument have permitted the observation of amino acid sequence-specific fragmentation of peptide ions and its dependence on the length of time that ions are stored.[28] Also, a continuous-flow MALDI-QIT/TOF instrument directly interfaced with high-performance liquid chromatography (HPLC) has been demonstrated by the Lubman group.[29]

Mass resolution is among the most important parameters describing mass spectrometer performance. However, reports on successful interfacing of the QIT with a TOF mass analyzer exhibit a wide discrepancy in values for mass resolution. For example, in the case of MALDI-generated ions the mass resolution [$m/\Delta m$ at the full width at half maximum intensity (FWHM)] on instruments using a reflectron time-of-flight (reTOF) mass analyzer, was reported in the range of $R = 200$–250 for ions of m/z 85–1350[28] and $R = 6200$ for m/z 1347.[27] The mass resolution on the same QIT/reTOF instrument interfaced with an ESI ion source varied from $R = 1000$ for m/z 462[30] to $R = 1700$–3000 for m/z 340–1200.[31] On another QIT/reTOF instrument a mass resolution of $R = 1200$ was reported for benzene.[32]

It is obvious that the mass resolution is a complex function of the experimental parameters which also depends on the instrument design. Hence it was the goal of this work to optimize the design of the QIT/reTOF instrument and study the dependence of the mass resolution on the parameters of the experiment. Since the distribution of the kinetic energy of ions extracted from the trap was shown to be very broad and we used no additional acceleration after ion extraction to shorten the length of the TOF section, a reflectron capable of focusing ions distributed over a broad range of energy was used. From among various types of broad energy reflectron mass analyzers described in the literature,[33–36] a simple parabolic reflectron was chosen in our design. The various aspects of operation of the QIT/TOF instrument with a parabolic reflectron are addressed in this paper, including the theory and simulation of the extraction of ions from an ion trap, the design of a parabolic reflectron, the modification of the geometry of the quadrupole ion trap used, the efficiency of the reflectron for focussing ions having a wide spread of kinetic energies, the dependences of mass spectral linewidth on extraction voltages, trapping r.f. voltage amplitude and phase of shutting down the r.f. voltage before the extraction, mass shift at various r.f. trapping voltage amplitudes and tandem mass spectrometry.

NUMERICAL SIMULATION

Extraction of ions from the ion trap

The initial condition for ions just prior to their extraction will have a strong effect on the quality of the ion beam after the extraction and, thus, on the sensitivity and the mass resolution of the instrument. The initial distribution of ions before extraction is affected by the presence of the helium buffer gas inside the trap. Normally the helium pressure is about 1 mTorr[1] and is used for cooling ions after their injection into the trap from an ion source as well as for collisional activation and fragmentation of ions in tandem experiments. As a result of collisions with helium molecules, the spatial distribution of ions about the center of the trap reaches equilibrium within a few milliseconds. In the pseudopotential approximation,[1] which neglects the micromotion of particles at the fundamental r.f. frequency, the equilibrium spatial distribution of ions before extraction is governed by the pseudopotential $\Phi(\rho, z)$ created by the r.f. electric field, where ρ and z are cylindrical coordinates. For evaluation purposes we consider a pure quadrupolar field and neglect the coulomb interaction between ions and approximate the pseudopotential well by a parabolic function with depths D_z and D_ρ in the axial z and radial ρ directions, respectively: $\Phi(\rho, z) = D_\rho(\rho/r_0)^2 + D_z(z/z_0)^2$, where r_0 is the radius of the ring electrode and z_0 is the displacement of the end-caps from the center. In this approximation the spatial distribution of ions is described by the function[37]

$$n(\rho, z) = N\left(\frac{2\pi kT}{e}\right)^{3/2}\left(\frac{{r_0}^2 z_0}{D_\rho D_z^{1/2}}\right)\exp\left[-\frac{e\Phi(\rho, z)}{kT}\right] \quad (1)$$

where $n(\rho, z)$ is the ion density, N is total number of ions in the trap, e is the ion charge, k is the Boltzmann constant and T is the ion temperature. The well depth D_z is determined by the r.f. voltage $V_{\text{r.f.}}$ (0-to-peak) and the Mathieu parameter q_z:[1,37]

$$D_z = \frac{q_z V_{\text{r.f.}}}{8} = \frac{eV_{\text{r.f.}}^2}{2m{r_0}^2\Omega^2} \quad (2)$$

where m is the ion mass, $\Omega = 2\pi f$ and f is the frequency of the r.f. field. The well depth in the radial direction is simply related to D_z when there is no d.c. voltage between the ring and end-cap electrodes: $D_\rho = D_z/2$.

Equations (1) and (2) were used to calculate the characteristic half-width δ_ρ of the ion spatial distribution in the ρ direction (Fig. 1), which we define as the distance at which the ion density drops by e times:

$$\delta_\rho = (kT/eD_\rho)^{1/2} r_0 \quad (3)$$

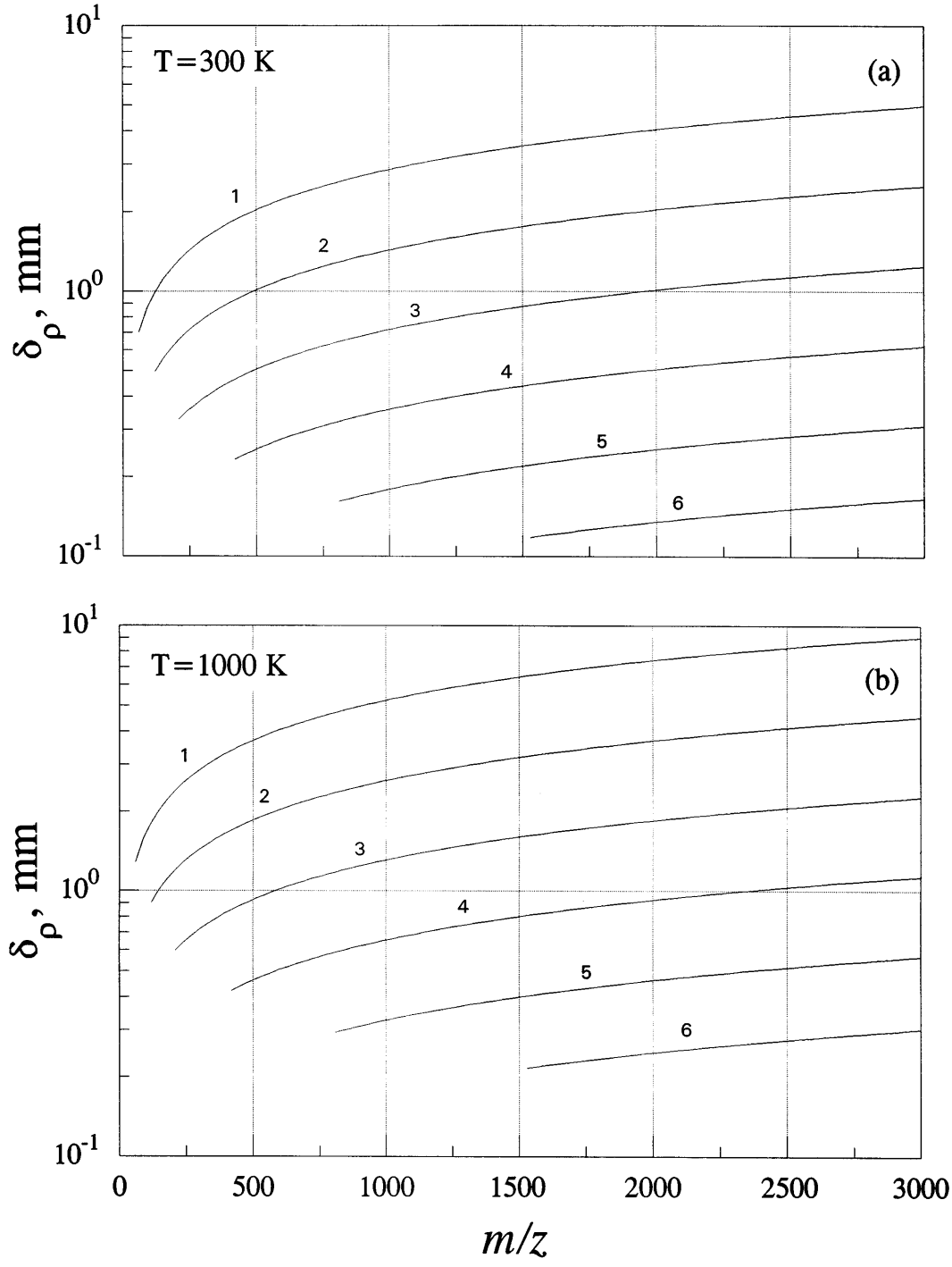

Figure 1. Typical size of ion cloud in the radial direction as a function of m/z for ion temperatures of (a) 300 and (b) 1000 K at different trapping voltages: (1) 250; (2) 500; (3) 1000; (4) 2000; (5) 4000; (6) 7500 V_{0-p}.

The calculations in Fig. 1 were made for two ion temperatures, $T = 300$ and 1000 K (the former is the room temperature and the latter is within the range of temperatures observed in the experiment[38,39]), and different trapping voltages, $V_{r.f.}$, from 250 (curve 1) to 7500 V_{0-p} (curve 6). The corresponding half-widths in the z direction are given by $\delta_z = \delta_\rho/2$. The value of δ_ρ in Fig. 1 is shown only for $q_z < 0.4$ at which the pseudopotential well approximation is valid.[1,37] The half-width δ_ρ determined by Eqn (1) is a good approximation for the evaluation of the radius of the hole in the end-cap electrode needed for ion extraction into the TOF stage. As one can see from the data in Fig. 1, there is a trade-off between the requirements of low-mass cut-off level and narrow ion distribution in the x–y plane for better extraction of ions into the TOF mass analyzer. For example, the optimal values of the r.f. voltage $V_{r.f.}$ for extraction of ions in the mass range up to m/z 2500–3000 in the standard ion trap lie between 1000 and 2000 V_{0-p}. The half-width δ_ρ for these values of voltage does not exceed 1.5–2 mm.

The main features of the process of ejecting ions into the TOF analyzer can be observed using the SIMION 3D ion trajectory program[40] as shown in Fig. 2 for a

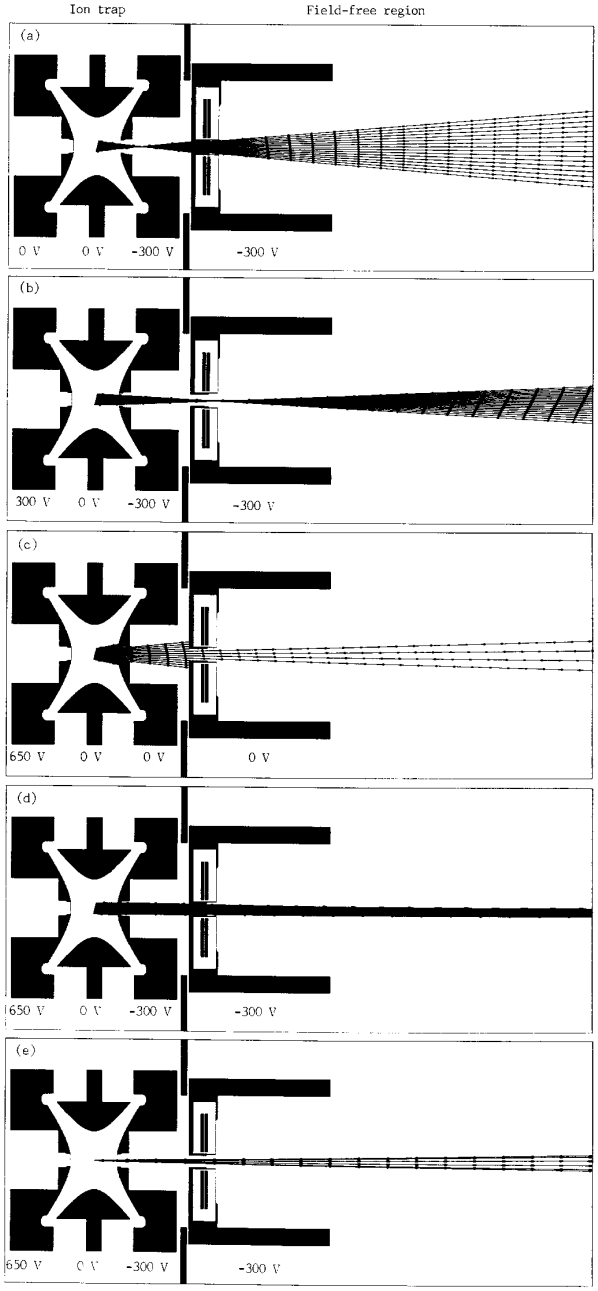

Figure 2. Divergence of ion beam at different extracting voltages. In cases (a)–(d), ions are spatially distributed and have zero initial velocity; in case (e), ions are located at the ion trap center and have an isotropic velocity distribution corresponding to a temperature of 1160 K.

standard ion trap geometry with 4 mm diameter holes drilled in the end-cap electrodes and covered by a mesh. The simulations are carried out for the actual aperture used in our experiment which includes a 4 mm diameter channel at the center of the microchannel plate (MCP) assembly for passing ejected ions into the TOF stage. The ions are injected into a field-free region and, thus, the angular focusing of the ion beam is due entirely to the field inside the trap. In Fig. 2(a)–(d) the ions initially have been spatially distributed near the center of the trap along the ± 0.5 mm axial and ± 1.8 mm radial intervals, but do not have initial kinetic energies. Ions in Fig. 2(e) are initially placed at the center of the trap and have initial kinetic energies of 0.1 eV (1160 K) and an isotropic velocity distribution. The calculations are shown for the case of m/z 3000 with time markers drawn every 2 μs. The trajectories (but not time markers) will be the same for ions of any mass provided their initial energies are the same. By adjusting the voltages on the end-caps one can achieve a nearly parallel beam at the trap exit for ions initially at rest [Fig. 2(d)].

In this case of Fig. 2(d) the voltage values differ from those used in experiments with attractive d.c. pulses [Fig. 2(a)] or symmetric voltage pulses on the end-caps[24–26] [Fig. 2(b)] and are in fact a combination of the repulsive [Fig. 2(c)] and symmetric [Fig. 2(b)] cases. For this reason the curved field inside the trap is intermediate between the repulsive case, in which the potential along the axis is nearly quadratic[24] and the symmetric case, in which the potential distribution along the trap axis is nearly linear. Because the field inside the trap works in the same manner as in a reflectron, the energy interval (which is due to the initial spatial ion distribution in the trap) focused by this curved field should be intermediate between that focused by linear extraction (first-order focusing) and quadratic extraction (which should be independent of energy or infinite-order focusing). (Here we are talking about the space focusing of ions along the axial direction as opposed to the angular focusing discussed in the previous paragraph.) The extraction field converts the initial spatial distribution of ions into a kinetic energy distribution at a particular focal point (or plane). In the linear case [Fig. 2(b)], this places the focal plane at a distance of $2z_0$ outside of the trap. For a quadratic case [Fig. 2(c)], the focal plane lies at the inner surface of the exit end-cap electrode. The curved field extraction shown in Fig. 2(d) converts the spatial distribution into an energy distribution at a plane outside the trap like that in the linear case [Fig. 2(b)] but closer to the exit hole in the end-cap.

Designing a parabolic reflectron

The focal plane outside the trap in Fig. 2(d) can be used as a focal plane for a reflectron. This approach is different from that used in previous work[3,14–16,22–32] where ions were additionally accelerated after extraction. The absence of the acceleration stage after extraction of ions from the trap allows one to avoid the negative effect of grids and field curvature (in the case of gridless designs for acceleration) on the sensitivity and the mass resolution. The width of the energy distribution of ions after the extraction is about the same as would be in the case if they were additionally accelerated; however, the average energy of ions is much less, making the contribution of energy spread to the final energy more significant. For example, from the size of the ion cloud before ejection $\delta_z = 1$ mm (Fig. 1) one can estimate that in the case of linear extraction [Fig. 2(c)] the difference in the kinetic energy of ions in the ion packet after extraction can reach 25% of the average energy. Such a large energy spread cannot be focused by a linear field reflectron because it provides only first-order focusing.[9] A broad energy focusing, or ideal, reflectron[33–36] should be used in this situation. From among designs available

in the literature a simple parabolic reflectron[33] was chosen in this work for broad energy focusing.

The problems associated with the construction of a parabolic (or quadratic-field) reflectron have been discussed earlier.[33,41] Among them is the fact that indefinite order focusing is achieved when there are no drift spaces, while such field-free regions are necessary in any practical design to accommodate ion lenses, detectors, etc. The length of the field-free spaces in our experimental configuration shown in Fig. 2(d) is equal to $L_f = 24$ mm and includes the distance from the focal plane formed after extraction of ions from the trap to the entrance grid of the MCP assembly and the small post-acceleration region inside this assembly (corrected for the inconstant ion velocity). While not ideal, the focusing remains very effective if the value of L_f is small in comparison with the length of the reflectron L_r and the potential $\phi^{(0)}$ along the z axis of the reflectron is chosen in the form[33]

$$\phi^{(0)} = \frac{\alpha}{2}(z + a)^2 + \beta \tag{4}$$

where $a = L_f/2$, $z = 0$ corresponds to the entrance grid of the MCP assembly and α and β are the constants defining the parabolic field.

Another problem in designing the parabolic reflectron results from the actual curvature of the electric field in the reflectron. The electric field must satisfy the LaPlace equation and, thus, the curvature exists both in the axial and transverse (or radial) directions. The curvature in the radial direction results in some dropping of the potential distribution along the radius, so that the potential at the central part of the reflectron is not equal to that of the lenses used for defining the parabolic field. This then limits the aperture which might be used in a parabolic reflectron as well as in designing the reflectron itself. This phenomenon was neglected in an early design[33] where the field was defined using a set of ring-like electrodes and thoroughly addressed in a later study.[41] In the latter case, a quadratic field inside the reflectron was defined by electrodes embedded in boundary printed-circuit boards. The voltage values on the electrodes corresponded to the boundary conditions defined by the LaPlace equation for a quadrupolar field.

Although the latter approach[41] is a general one, its application to a commonly used design in which a reflectron is composed of numerous ring-like electrodes is ambiguous because of the small thickness of the electrodes and the flatness of the end electrodes in the electrode structure. For this reason we decided to use a best fit method for adjusting the potential on the electrodes to achieve a potential along the axis of the reflectron as close to the parabolic function as possible. A simple criterion of the minimum mean square deviation was used to find the best value of voltage V_i on the ith electrode ($i = 1, \ldots, n$, where n is the number of the electrodes) which for the discrete presentation of the parabolic potential (4) $\phi_k^{(0)}$ can be written as

$$F(V_i) = \sum_{k=1}^{N} \left\{ \sum_{i=1}^{n} [V_i \Phi_k^{(i)}] - \phi_k^{(0)} \right\}^2 \tag{5}$$

where $k = 1, \ldots, N$, where N is the number of discrete grid points along the reflectron axis where the potential is monitored, $\Phi_k^{(i)}$ is the potential generated by the ith electrode at the grid point k when the potential on the ith electrode is equal to unity while the potentials on all other electrodes are equal to zero. The function (5) can be rewritten in the form

$$F(V_i) = \sum_{i,j=1}^{n} A^{(ij)} V_i V_j - 2 \sum_{i=1}^{n} B^{(i)} V_i + C \tag{6}$$

where

$$A^{(ij)} = \sum_{k=1}^{N} \Phi_k^{(i)} \Phi_k^{(j)} \tag{7}$$

$$B^{(i)} = \sum_{k=1}^{N} \Phi_k^{(i)} \phi_k^{(0)} \tag{8}$$

$$C = \sum_{k=1}^{N} \phi_k^{(0)} \phi_k^{(0)} \tag{9}$$

The minimum of function (6) and the voltages V_i can be found by solving the system of the algebraic equations $\delta F/\partial V_i = 0$ ($i = 1, \ldots, n$). However, we found that for large n the convergence of numeric methods normally used for solving this system is very slow. For this reason, we decreased the number of unknown variables by looking for the voltages on the electrodes in the polynomial form:

$$V_i = \sum_{l=1}^{S} \gamma_l z_{(i)}^{l-1} \tag{10}$$

where $z_{(i)}$ is the coordinate of the ith electrode, γ_l is the expansion coefficient, $l = 1, \ldots, S$, $S \ll n$. Substituting V_i in the function (6) for (10) and differentiating over γ_l one can obtain the conditions for the minimum of the function (6):

$$\sum_{l=1}^{S} a^{(lm)} \gamma_l = b^{(m)} \tag{11}$$

where $m = 1, \ldots, S$ and

$$a^{(lm)} = \sum_{i,j=1}^{n} A^{(ij)} z_{(i)}^{l-1} z_{(j)}^{m-1} \tag{12}$$

$$b^{(m)} = \sum_{i=1}^{n} B^{(i)} z_{(i)}^{m-1} \tag{13}$$

In practice, the arrays of the potentials $\Phi_k^{(i)}$ were found using the SIMION 3D program[40] and, thus, the grid presentation in Eqns (5) and (7)–(9) coincided with that in SIMION 3D. The coefficients $a^{(lm)}$ and $b^{(m)}$ were calculated and then the expansion coefficients were found by solving the system (11) using an in-house written program.

EXPERIMENTAL

Quadrupole ion trap

Experiments were carried out using an extensively modified Finnigan MAT (San Jose, CA, USA) ion trap detector (ITD) shown in Fig. 3. Many of the instrument features have been described in detail elsewhere.[20,42,43] MALDI using the third harmonic ($\lambda = 355$ nm) laser pulse of 4–6 ns duration from a Continuum (Santa

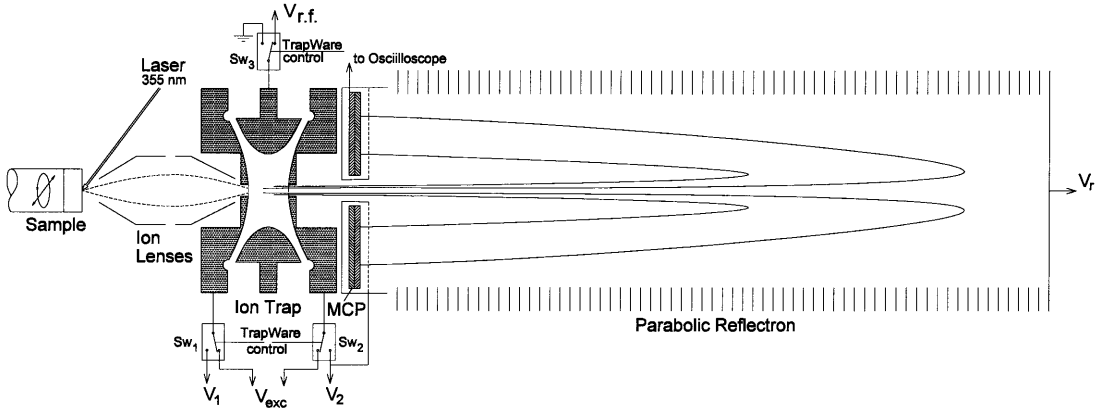

Figure 3. Schematic diagram of quadrupole ion trap/time-of-flight instrument with a parabolic reflectron.

Clara, CA, USA) Minilite-10 Q-switched Nd:YAG laser was used for the production of ions in an external source.[43] Other instrument features include increased efficiency for trapping MALDI ions by increasing the r.f. voltage,[44] a broadband excitation technique designed for the unit resolution ion isolation in the range up to 1600 Da using 'stretched-in-time' excitation waveforms[20] and pulsed introduction of heavy gas used in MS/MS experiments for improving collision-induced dissociation (CID) efficiency and to allow a low-mass cut-off level for fragment ions analyzed.[42] The ion trap assembly was placed inside a two-section coffin vacuum chamber in which the ion trap and TOF sections were pumped differentially by two turbomolecular pumps [Models TMP 150 (Leybold, Export, PA, USA) and TPH 330 (Balzers, Hudson, NH, USA)]. The hole in the exit end-cap electrode served as a conductance limit between two vacuum sections. The pressure was about 10^{-3} and 2×10^{-6} Torr in the QIT and TOF sections, respectively.

The trapping r.f. voltage amplitude was controlled externally using 12-bit analog outputs from a National Instruments (Austin, TX, USA) Lab PC+ multifunction plug-in board connected to the computer. A.c. voltage and broadband waveforms applied to the end-cap electrodes for the excitation and isolation of ions inside the trap were generated by a waveform synthesizer composed of two Quatech (Akron, OH, USA) WSB-100 plug-in boards with an on-board WSB-A12M 12-bit resolution analog module connected to the computer. Twelve bits of each point of the WSB-100 64-kpoint, 16-bit memory were used to generate the analog broadband signal while the other 4 bits were used as digital lines to control external devices. The procedure for designing the excitation broadband waveforms was described earlier.[20] TrapWare software (designed in-house) was used for controlling the instrument and additional hardware.[20,45] TOFWare, a Windows-based program available from ILYS Software (Pittsburgh, PA, USA), was used for data processing and plotting.

Modification of ion trap electrodes

The geometry of the standard ITD electrodes was modified to facilitate the ejection of the ions into the TOF stage. The exit end-cap electrode was replaced by one identical with the entry end-cap. The holes in both end-caps were increased from 1.2 to 4 mm diameter and covered by a nickel mesh (118 lines per inch, 89% transparency) manufactured by Buckbee-Mears (St Paul, MN, USA). To compensate for changes in the electric field generated by the ion trap electrode assembly after modification, the end-caps were stretched by 1.9 mm (from the original, already stretched distance of 15.6 mm[1]). The distance between the end-cap electrodes was chosen to have near the center of an ion trap the same ratio of the octopolar field term to that for the quadrupolar field before and after modification. The harmonic analysis was made numerically using the SIMION 3D program and software written in-house. The octopolar field term near the axial region of the ion trap was about 1.6% of that for the quadrupolar field (multipole components were analyzed for the axial region at the interval of ± 4 mm from the center). Keeping the value of the octopolar field is important for ion resonant excitation methods, including a broadband excitation technique reported earlier,[20] to work properly in the modified ion trap. These methods are vital for isolation of ions in the trap for subsequent MS/MS experiments.

The approach of stretching further the distance between the end-cap electrodes was verified in experiments in which the trap was operated in normal mode as a stand-alone mass spectrometer using resonant ejection of ions to obtain mass spectra[1,45] (in these experiments the reflectron in Fig. 3 was replaced by an electron multiplier for ion detection). The mass resolution at m/z 1141 (protonated molecules of gramicidin S) was about 3500 in the ion trap mass spectrometer with the standard electrode geometry at the normal distance of 15.6 mm between end-caps and the mass scan rate 1000 Da s^{-1},[43] while under the same conditions but with the end-cap electrodes having 4 mm diameter holes covered by the mesh, the mass resolution does not exceed a few hundred so that no isotopic structure is seen. When the distance between the modified end-cap electrodes is increased by 1.9 mm then the mass resolution recovers to about 2500.

Parabolic reflectron

The detector assembly mounted near the exit end-cap electrode had a 4 mm hole for passing ions ejected from the trap to the reflectron (Fig. 3). A Chevron micro-

channel plate assembly (Galileo, Sturbridge, MA, USA) having a 25 mm diameter working area with a centered 6.4 mm diameter hole was used for ion detection. Before detection ions were post-accelerated up to 2.5–3 keV in a distance of about 2 mm between the detector assembly entrance grid (118 lines per inch, 89% transparency) and the MCP. The signal from the detector was recorded by a LeCroy (Chestnut Ridge, NY, USA) Model 9400A digital oscilloscope. It is important to note that ions pass through grids only twice during their flight time and that discontinuities in the electric field at the first grid in the exit end-cap electrode are minimal, so that the effect of the grids on ion scattering and mass resolution is minimized.

The parabolic field inside the reflectron was built using 124 ring-like 50.8 mm diameter electrodes having an inner diameter of 33–38 mm diameter. The ring electrodes were equally spaced to form a coaxial reflectron of total length of 447 mm. The reflecting d.c. potential V_r was applied to the end flat electrode while the voltages on other electrodes were established using a resistive divider.

QIT/reTOF interface

The divergence of the ion beam according to the data presented in Fig. 2 can be controlled by varying the extraction voltages on the end-cap electrodes with the best voltage configuration shown in Fig. 2(d). Thus, a QIT/reTOF interface was built without the focusing ion lenses normally used to control ion beam divergence. This also saved the space for closer connection of the QIT and TOF parts of the instrument because the parabolic reflectron does not permit a long field-free region and resulted in a simple compact design shown in Fig. 3 where the coaxial parabolic reflectron is directly attached to the ion trap via a thin isolating spacer.

During the trapping period, the trapping voltage $V_{\text{r.f.}}$ from the ITD r.f. generator was applied to the ring electrode and broadband excitation voltage V_{exc} from the WSB-100 waveform generator could be applied to the end-cap electrodes for ion isolation or activation. Before extraction of ions from the trap, the trapping r.f. voltage on the ring electrode was shut down to zero (ground) for a period less than 100 ns using a laboratory-built high voltage switch (Sw_3 in Fig. 3). Then, after a variable time delay, extraction pulses with pulse rise times <25 ns and about 20 μs duration were applied to the end-cap electrodes using a modified Directed Energy (Fort Collins, CO, USA) Model GRX-1.5K-E pulsers working as high-voltage switches (Sw_1 and Sw_2 in Fig. 3). Thus, during extraction of ions the ring electrode was grounded and the d.c. voltages V_1 and V_2 (up to ± 1500 V) were applied to the end-caps. The timing for the ion extraction can be precisely synchronized with the r.f. 1.1 MHz and line 60 Hz voltage cycles.[46] The extraction signal also triggered the oscilloscope for recording a mass spectrum.

Operational procedures

The entire operation of the MALDI-QIT/reTOF instrument was controlled using TrapWare software. A typical operational procedure included the following: formation of ions using the laser pulse; injection and trapping of ions in the trap using an increasing r.f. voltage;[44] a period of cooling via collisions with helium molecules (50 ms) at an r.f. voltage of about 1875 V_{0-p}; ramping of the r.f. voltage to the pre-ejection level; ejection of ions into the reTOF stage; and recording the signal with 10 ns resolution using the digital oscilloscope. The mass spectra from about 100 single laser shots were summed using the oscilloscope averaging option to obtain the final mass spectrum which was then transferred via an instrumental GPIB interface to the IBM computer for further processing and plotting. In tandem experiments additional stages were inserted after trapping and cooling ions that included the following: isolation of the precursor ions using a broadband excitation technique for ejection of unwanted ions;[20] injection of xenon gas at a pressure of about 1 mTorr for a time of about 100 ms using a pulsed gas valve;[42] CID of the isolated ions using a sustained off-resonance irradiation (SORI) method[47,48] for excitation of ions in the bath of the xenon molecules (25–50 ms);[42] and pumping out the xenon gas from the QIT vacuum section for about 100 ms. The frequency of SORI sinusoidal excitation was about 5% lower than the resonant frequency of ions and its amplitude was about 2.2 V_{0-p}.

α-Cyano-4-hydroxycinnamic acid (Aldrich, Milwaukee, WI, USA) was used as the MALDI peptide matrix. It was prepared as a saturated solution in 1:1 ethanol–water, deposited on the stainless-steel probe in an amount of 10–20 μl and dried in a flow of air at room temperature. Aqueous solutions of about 10 pmol substance P or gramicidin S (Sigma, St Louis, MO, USA) in the amount of 3–4 μl were deposited on the matrix and dried in the vacuum. Each sample was used to produce thousands of single laser shot spectra by moving the sample probe within an area of ~ 20 mm^2.

RESULTS AND DISCUSSION

Efficiency of the reflectron for focusing ions having a wide spread of energies

The SIMION 3D program was used to evaluate the focusing properties of the reflectron. The instrument electrode structure was approximated with 0.2 mm accuracy. The electric potential field during extraction of ions is shown in Fig. 4 (in this simulation no acceleration voltage was applied to the MCP). The potential distribution inside the reflectron was calculated using the best fifth-power polynomial fitting method described in the Numerical Simulation section. The extraction voltage configuration in Fig. 4 is similar to that shown in Fig. 2(d) and the reflecting potential V_r is about 1.33 times larger than the potential at the center of the trap during extraction. Thus, after the extraction, ions located initially at the center of the trap penetrate the reflectron to the extent of $\sim 75\%$ of its total length.

The capability of the reflectron to focus ions having a broad range of initial energies is illustrated by data in Fig. 5, where relative variations in the ion time-of-flight

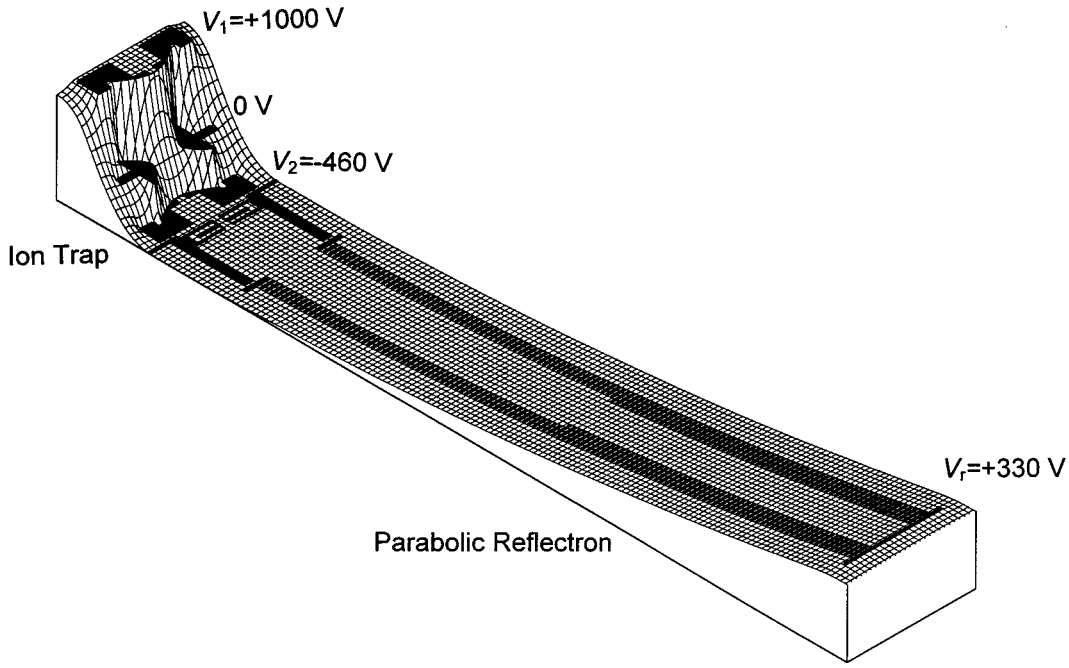

Figure 4. Typical distribution of the potential extracting and reflecting fields in the QIT/reTOF instrument.

$\delta t/t_{TOF}$ (where t_{TOF} is the ion total time-of-flight in the reflectron) are shown as a function of the ion initial relative kinetic energy $\varepsilon/\varepsilon_{max}$ at the entrance of the reflectron (ε_{max} is the maximum entrance kinetic energy at which ions are still reflected in the reflectron). The data are the results of simulations in which all potential fields were maintained at the same value while the initial kinetic energy of ions located at the reflectron focal plane was varied. From the data in Fig. 5 one can conclude that theoretical mass resolution of the reflectron ($R = t_{TOF}/2\delta t$) can reach 5000 for ions having an initial kinetic energy distribution lying within 50% of the maximum reflectron energy ε_{max}. A surge in time-of-flight deviations is observed for energies below $0.44\varepsilon_{max}$. This energy corresponds to a 66% depth of the penetration of ions into the reflectron. This depth is close to the point of the transition in the ring electrode hole diameter from 38 to 33 mm (see Fig. 4). A surge for energies higher than $0.93\varepsilon_{max}$ can be explained by the influence of the flat end electrode.[41]

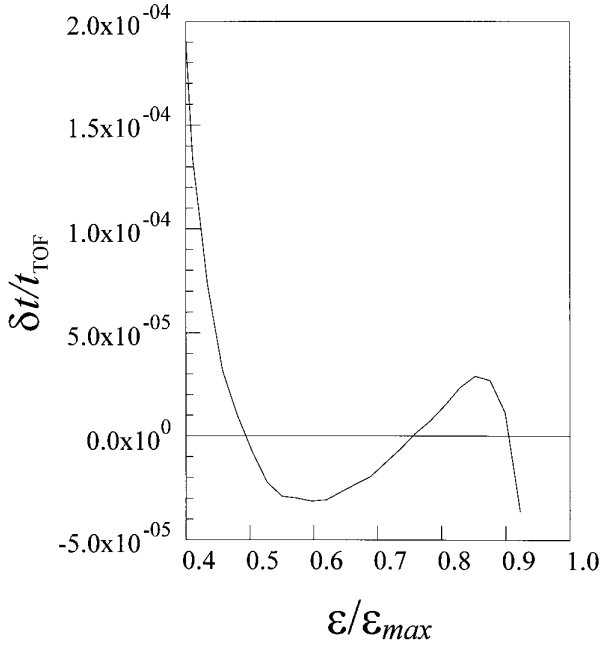

Figure 5. Relative variations of time-of-flight of ions in the parabolic reflectron as a function of initial relative kinetic energy (ε_{max} is the maximum kinetic energy at which ions are still reflected by the reflectron).

Dependence of mass spectral linewidth on extraction voltage

The mass spectral lines of fragment and matrix ions in the range from m/z 116 to 813 in MALDI mass spectra of gramicidin S shown in Fig. 6(a) [Fig. 6(b) and 6(c) will be discussed later] were used to study the dependence of the mass resolution of the instrument on different experimental parameters. The total time-of-flight t_{TOF} for sodium cationized ions of gramicidin S at the extraction voltages shown in Fig. 2(d) is about 160 μs.

The dependence of linewidth δt (according to FWHM criteria) on m/z at different extraction potentials is shown in Fig. 7. Every point in Fig. 7 (and subsequently Figs 8–11) represents the average of the linewidth values from three different mass spectra obtained at the same conditions with the estimated error not exceeding 8%. The extraction voltages used in these experiments were similar to the configuration shown in Fig. 2(d) and are specified in Table 1 where the strength of the electric field at the center of the trap E_0 and the reflecting potential V_r are also shown. Other variable parameters were fixed in these experiments and among them are: the trapping voltage before extraction $V_{r.f.} = 1875\ V_{0-p}$; the r.f. phase at which the r.f. voltage was shut down

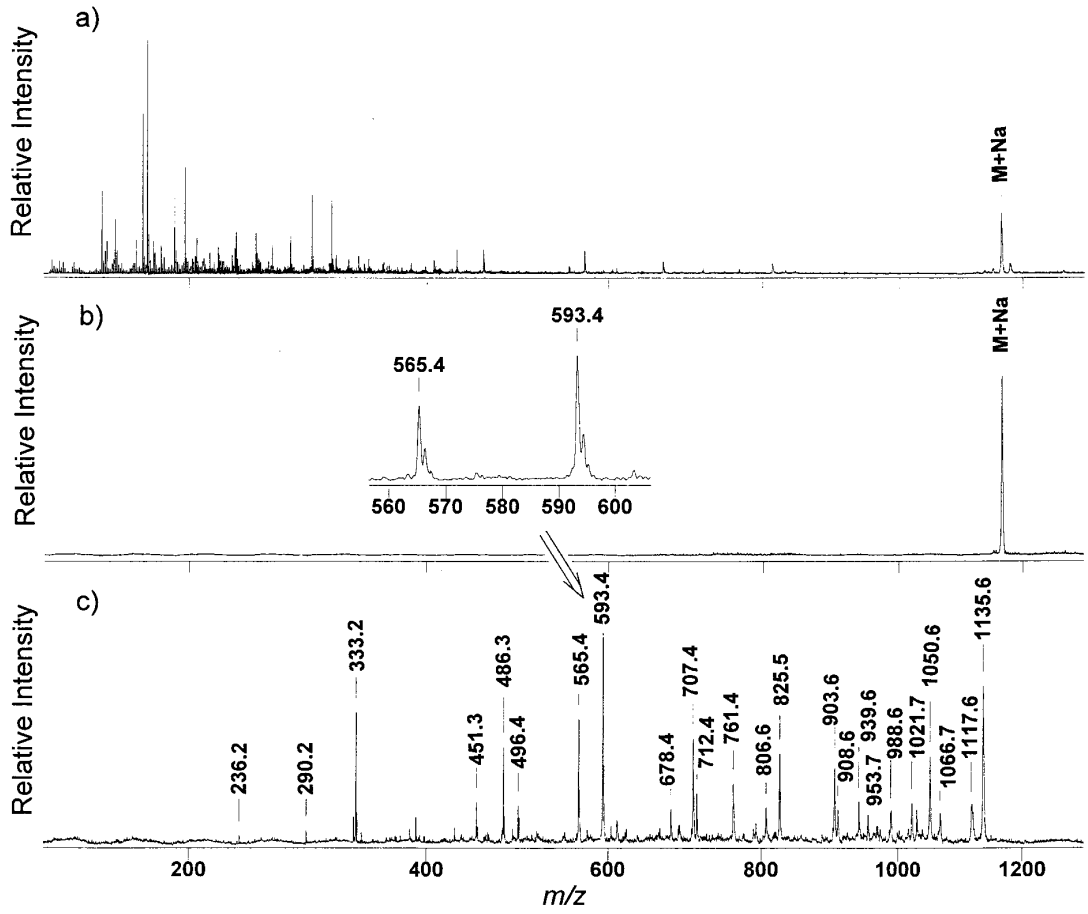

Figure 6. MALDI-QIT/reTOF mass spectra of gramicidin S (M_r = 1141.5 Da): (a) after injection and storing for 50 ms; (b) after isolation of sodium cationized ions using a broadband excitation technique; (c) after fragmentation of the isolated ions via collisions with xenon molecules using a SORI excitation method.

$\theta_{r.f.} = 40°$ ($\theta_{r.f.} = 0°$ corresponds to zero increasing r.f. voltage); and the time delay between shutting down the r.f. voltage and the application of the extraction voltages on the end-caps $t_d = 200$ ns. No dependence of the linewidth on the extraction delay time t_d was observed in this work when the value of t_d was varied from 0 to 2 μs (the data are not shown). Additionally, the absolute and relative intensity of mass spectral lines was about the same when the value of t_d was between 0 and 500 ns. At larger delay times the absolute intensities began to drop and that drop was much faster for lighter ions. Such behavior is in agreement with estimations for the time of leaving the trap by ions after shutting down the trapping voltage.

One can observe relatively smooth behavior of the linewidth on the ion mass in the range of higher masses (>300 Da) and beat-like behavior at lower masses which is more pronounced at lower extraction voltages. The linewidth behavior observed cannot be attributed to the time resolution limit (10 ns) used for digitizing in the experiments because any errors due to the process of digitizing would be more likely to be observed in Case 5 than in Case 1 in Fig. 7 where the beat-like structure is most pronounced. There is a good correlation between the region of the transition from the beat-like behavior to the smooth dependence and the limits of validity of the pseudopotential approximation for describing the motion of ions in a trap $q_z < 0.4$ (the

Table 1. Extraction and reflectron parameters used in experiments

Case No.	Repulsive extraction voltage, V_1 (V)	Attractive extraction voltage, V_2 (V)	Electric field strength at the trap centre, E_0 (V cm^{-1})	Reflectron voltage, V_r (V)
1	288.9	−133.3	175.2	96.3
2	433.3	−200	262.7	144.4
3	650	−300	394.1	216.7
4	866.7	−400	525.5	288.9
5	1000	−461.5	606.3	333.3

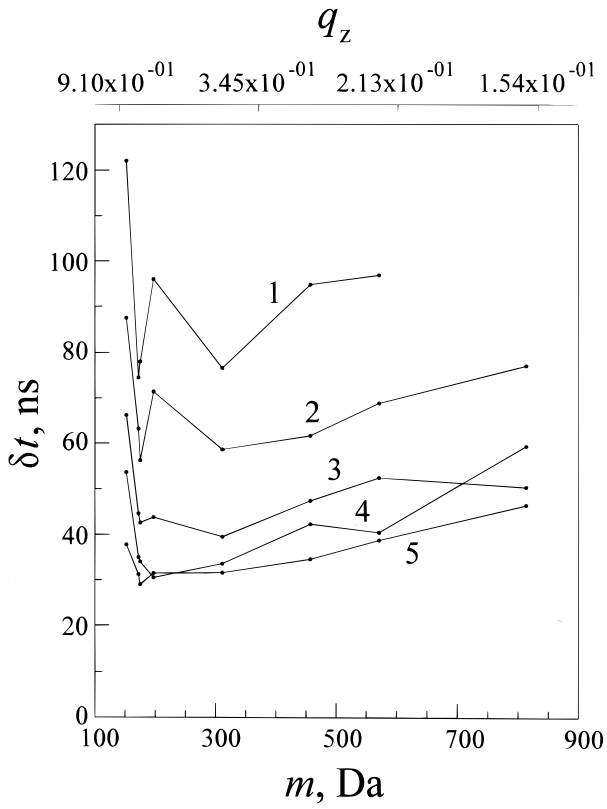

Figure 7. Dependence of mass spectral linewidth on ion mass at different extraction potentials (the curve numbers correspond to Case numbers in Table 1).

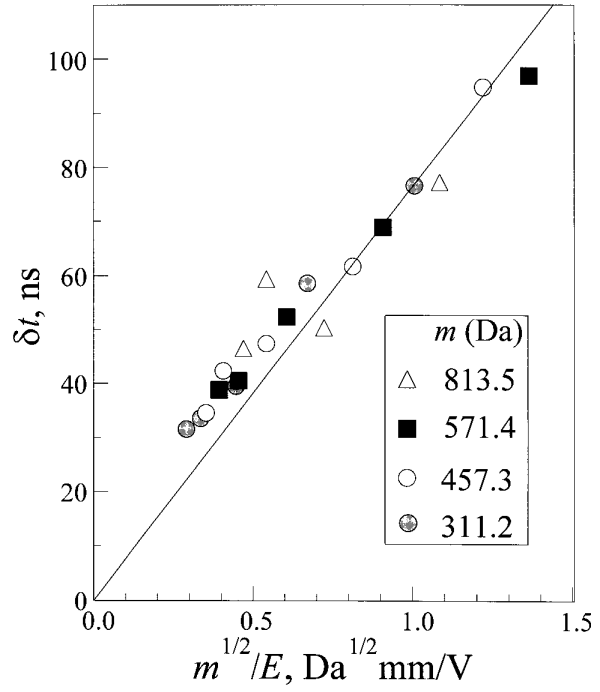

Figure 8. Dependence of mass spectral linewidth of ions shown at $q_z < 0.35$ in Fig. 7 on the parameter $m^{1/2}/E$.

q_z axis is shown at the top of Fig. 7). Thus, one can suggest that the beat-like behavior is due to the large amplitude of ion motion at the fundamental r.f. frequency at $q_z > 0.4$ and the linewidth in this case strongly depends on the phase at which the r.f. voltage is shut down. Experiments to study the dependence of linewidths on the phase of shutting down the r.f. voltage are described below.

One can also suggest that the mechanism for line broadening at $q_z < 0.4$ is different from that at $q_z > 0.4$. It is a good approximation that due to the presence of buffer gas the ion velocity and space distribution at $q_z < 0.4$ is the equilibrium one and is described by pseudopotential well parameters and temperature T.[37] If extracted ions initially have some velocity v_z in the z direction then the line broadening is determined by the so-called "turn-around' time,[9,10] which in our case is equal to

$$\delta t = \frac{2mv_z}{eE} = 2.355\sqrt{kT}\,\frac{\sqrt{m}}{eE} \qquad (14)$$

where E is the strength of the electric field during extraction and the factor 2.355 is due to the FWHM definition of the linewidth. The mass resolution in the case when the linewidth is determined by Eqn (14) does not depend on the ion mass because the total ion flight time is also proportional to the square root of the mass. The data presented in Fig. 7 for $q_z < 0.35$ are shown in Fig. 8 as a plot in $\delta t - m^{1/2}/E$ coordinates using the data in Table 1 for the electric field strength in the center of the trap. One can observe that the dependence of δt on $m^{1/2}/E$ is the same for all masses and close to linear as is predicted by Eqn (14). The temperature of ions in the trap can be calculated from the data in Fig. 8: $T = 1180 \pm 160$ K (solid line in Fig. 8) that correlates with that measured by a "chemical thermometer" method.[38,39]

Dependence of mass spectral linewidth on the trapping r.f. voltage

Given the correlation revealed in Fig. 7 between the behavior of the mass linewidth and the value of the Mathieu parameter q_z, the dependence of the linewidth δt on the ion mass for different trapping voltages $V_{\text{r.f.}}$ is presented in Fig. 9 against q_z. In these experiments the extraction voltage parameters corresponded to Case 2 in Table 1, the r.f. voltage was shut down at the phase $\theta_{\text{r.f.}} = 40°$ and the extraction time delay $t_d = 400$ ns.

The dependence of δt on q_z in Fig. 9 is monotonic at low values of q_z (<0.3–0.4) and highly irregular at higher q_z and is consistent with our previous observations in Fig. 7. It is also clear that the dependence of δt on q_z at higher q_z values is not well described by the data in Fig. 9. This is probably due to the nature of processes occurring at higher q_z values that require additional study.

Similarly to those in Fig. 7, the data at low values of q_z can be processed in terms of the $\delta t - m^{1/2}/E$ dependence which is shown in Fig. 10. One can see that the ion temperature in not constant in these experiments and there is some correlation between the rise of the temperature from about 1250 to 1690 K (dashed lines in Fig. 10) and the increase of the trapping voltage $V_{\text{r.f.}}$. The average ion temperature determined from all data presented in Fig. 10 is 1440 ± 180 K (solid line in Fig. 10).

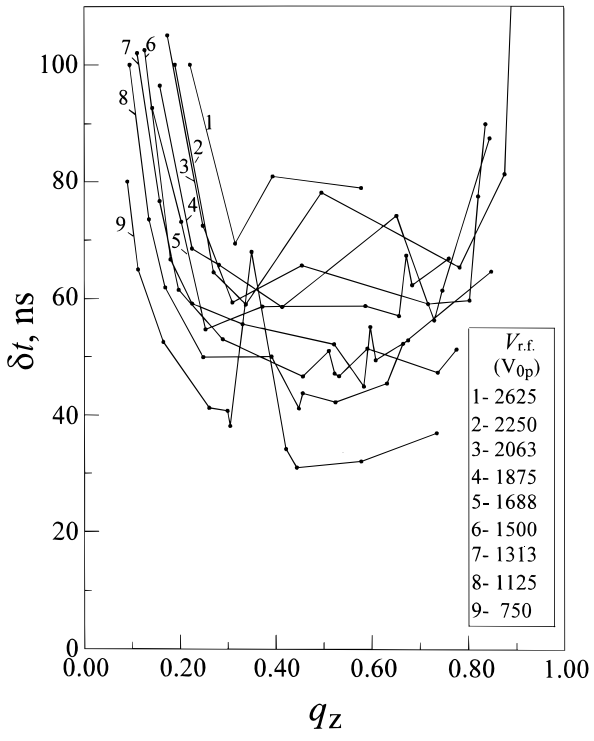

Figure 9. Dependence of mass spectral linewidth on the q_z value of ions at different trapping voltages before ion extraction.

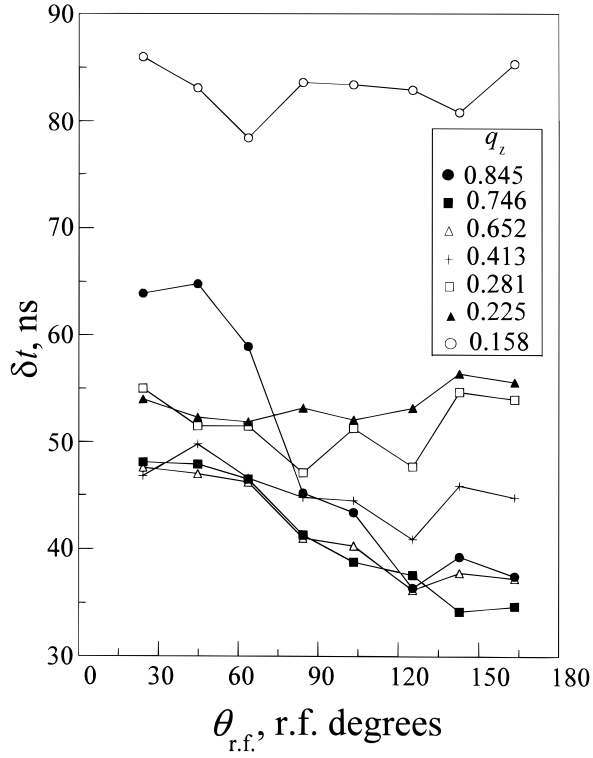

Figure 11. Dependence of mass spectral linewidth on the phase $\theta_{r.f.}$ of shutting down the r.f. trapping voltage before ion extraction at different q_z values.

Dependence of mass spectral linewidth on the extraction r.f. phase

The dependence of the linewidth δt on the extraction r.f. phase $\theta_{r.f.}$ is shown in Fig. 11. The high-voltage switch (Sw_3 in Fig. 3) used in the instrument allowed one to vary the phase of shutting down the r.f. voltage between 0 and 180° and, thus, the data for positive phases only are presented in Fig. 11. In these experiments the extraction voltage parameters corresponded to Case 3 in Table 1, the r.f. voltage $V_{r.f.}$ before the extraction was 1875 V_{0-p} and the extraction time delay $t_d = 400$ ns. The dependences in Fig. 11 are shown for ions at different q_z values that correspond to ions of different mass (for example, m/z 311.2 corresponds to $q_z = 0.225$). As one would expect from the above data in Figs 6–10, no or a small dependence on the extraction phase is observed at low values of q_z (0.158–0.281) and the linewidth changed by 50 ns for $q_z = 0.845$.

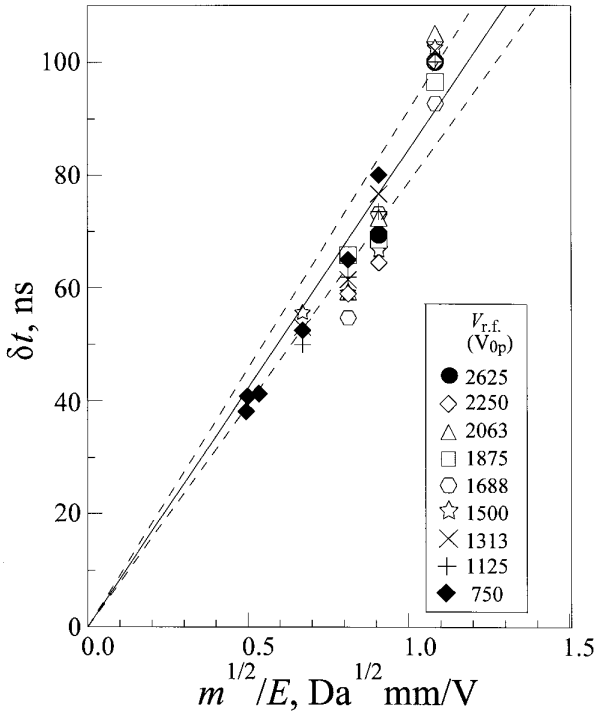

Figure 10. Dependence of mass spectral linewidth of ions shown at $q_z < 0.35$ in Fig. 9 on the parameter $m^{1/2}/E$.

In the simplest model presented by Eqn (14) in which the velocity v_z in the axial direction is determined by ripple micromotion (microoscillations) of ions at the frequency of the r.f. field, the minimum linewidth corresponds to the velocity of microoscillations equal to zero, i.e. to $\theta_{r.f.} = 90°$, that has some but not full correlation with the data presented in Fig. 11. The velocity of ripple microoscillations of ions at the drive r.f. frequency alone cannot account for irregular variations in the linewidth at higher q_z shown in Fig. 9 because these microoscillations are coherent for all ions inside the trap. Hence other possible reasons should be taken into account to explain this behavior. One such explanation may be related to a strong coupling of ion motion at the drive r.f. and secular frequencies at high q_z values so that they cannot be considered separately.[1] The resulting motion of ions can result in a strong asymmetric spatial and velocity distribution of ions inside the trap before extraction that can depend on ion mass. The combination of different temporal components of

ion kinetic energy which depends primarily on the r.f. trapping voltage amplitude and the effect of coupling r.f. and secular motions on ion velocity and spatial distributions may be responsible for complex behavior of the line width in Figs 7 and 9 at higher q_z values.

Mass shift at different trapping r.f. voltages

The results for systematic apparent mass shifts observed for different ions when the r.f. voltage is varied are shown in Fig. 12. In these experiments the same calibration curve was used for ion mass determination while the trapping voltage before extraction was changed. The extraction voltages corresponded to Case 3 in Table 1, the r.f. voltage was shut down at the phase $\theta_{\text{r.f.}} = 40°$ and the extraction time delay $t_d = 400$ns. The maximum variation in the apparent mass position of low-mass ions (m/z 172.05 and 197.1) corresponds to 50–55 ns and is close to that observed for the linewidth of these ions (see Figs 7 and 9). The maximum change in mass position for high-mass ions in Fig. 12 (m/z 571.45 and 813.5) corresponds to 28–33 ns, which is normally much less than the linewidths for these ions.

Low masses in Fig. 12 are associated with high values of q_z in Figs 7 and 9 and one can therefore assume that similar mechanisms are responsible for both the complex behavior of the linewidth at high q_z and the apparent mass shift phenomenon which is most pronounced for low-mass ions. However, the dependence of the apparent mass shift on the r.f. voltage is not as irregular as that for the linewidth. As one can see in Fig. 1, the effect of the r.f. voltage variations on the size of the ion cloud in the trap is most pronounced for the lightest ions. It is possible that the ion space distribution behavior alone can explain the apparent mass shift phenomena in Fig. 12 while both the ion spatial and velocity distributions should be taken into account for explanation of the complex behavior of the linewidth at high q_z values. The effects of ion spatial and velocity distributions on QIT/TOF performance have already been discussed in the literature.[8,23,32,49] In the absence of buffer gas, the fluctuations of the ion kinetic energy which are due to motion of the ion cloud along the trap axis resulted in a strong dependence of ion time-of-flight, intensity and mass resolution on the extraction phase.[32,49] Similar behavior for the intensity and mass resolution was observed in a study with collisional relaxation before ion extraction,[23] but these experiments were carried out without shutting down the r.f. voltage before extraction. In our experiments, no changes in linewidths were observed when the pressure of the buffer helium gas was increased or decreased fourfold.

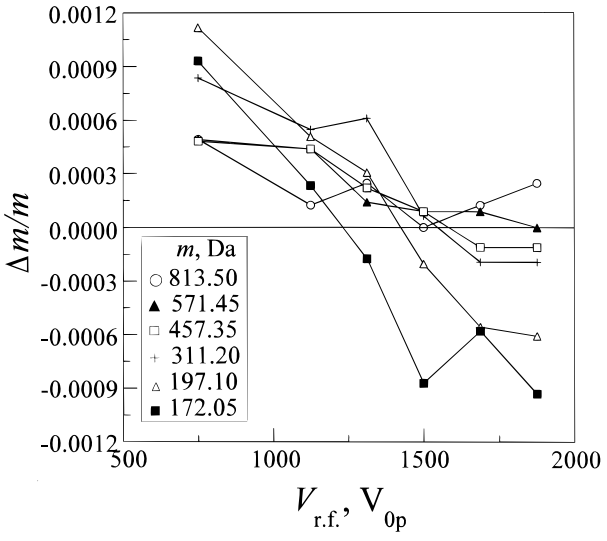

Figure 12. Variations of the relative apparent mass shift for different ions as a function of trapping voltage before extraction.

Tandem mass spectrometry

One example of CID mass spectra is shown in Fig. 6, where the spectra after trapping MALDI ions of gramicidin S using an increasing r.f. voltage[44] [Fig. 6(a)], isolating sodium cationized ions using a broadband excitation technique[20] [Fig. 6(b)] and fragmenting using injection of xenon molecules for increasing CID efficiency[42] [Fig. 6(c)] are presented. Another example is shown in Fig. 13 for protonated molecules of substance P. The spectra were obtained for the extraction voltages corresponding to Case 5 in Table 1, an r.f. voltage of 1875 V_{0-p} and shut down at the phase $\theta_{\text{r.f.}} = 40°$ and the extraction time delay $t_d = 400$ ns.

The successful isolation of the precursor ions is an important step in CID experiments and as one can see in Figs 6(b) and 13(b) this is possible after significant modification of the geometry of ion trap electrodes. As shown in the insets in Figs 6 and 13, the mass resolution is equal to ~1100 in both cases. The mass resolution remains about the same for all masses higher than ~300 Da, which is in agreement with Eqn (14) and is normally unpredictable (but lower) for lower masses where $q_z > 0.4$. According to Eqn (14), the resolution can be improved by increasing the extraction field but the improvement will be moderate because the mass resolution is proportional to the square root of the extraction field strength (in our case the time-of-flight is inversely proportional to the square root of the extraction potential). A mass resolution higher than 1400 was observed when the extraction voltages were increased to $V_1 = 1500$ V and $V_2 = -692$ V (data not shown). The values observed for the mass resolution correspond to the ion temperatures inside the trap in the range $T = 1180$–1690 K measured in this and other work.[38,39] Similar values for the mass resolution in QIT/reTOF instrument were obtained in some other experiments[30,32] but much lower[28] or much higher [23,31] values have also been reported in the literature. There is no basis for reconciling the extremely large difference between the values for the mass resolution obtained in this work and that reported by the Lubman group[23] ($R = 6200$).

Two more papers[50,51] on the topic of this work have been published since this paper was submitted for publication. A simulation of the ion extraction process was performed in the first.[50] Although the trapping r.f. voltage was not varied in the simulation (it is not even specified), the data for the linewidths obtained in the

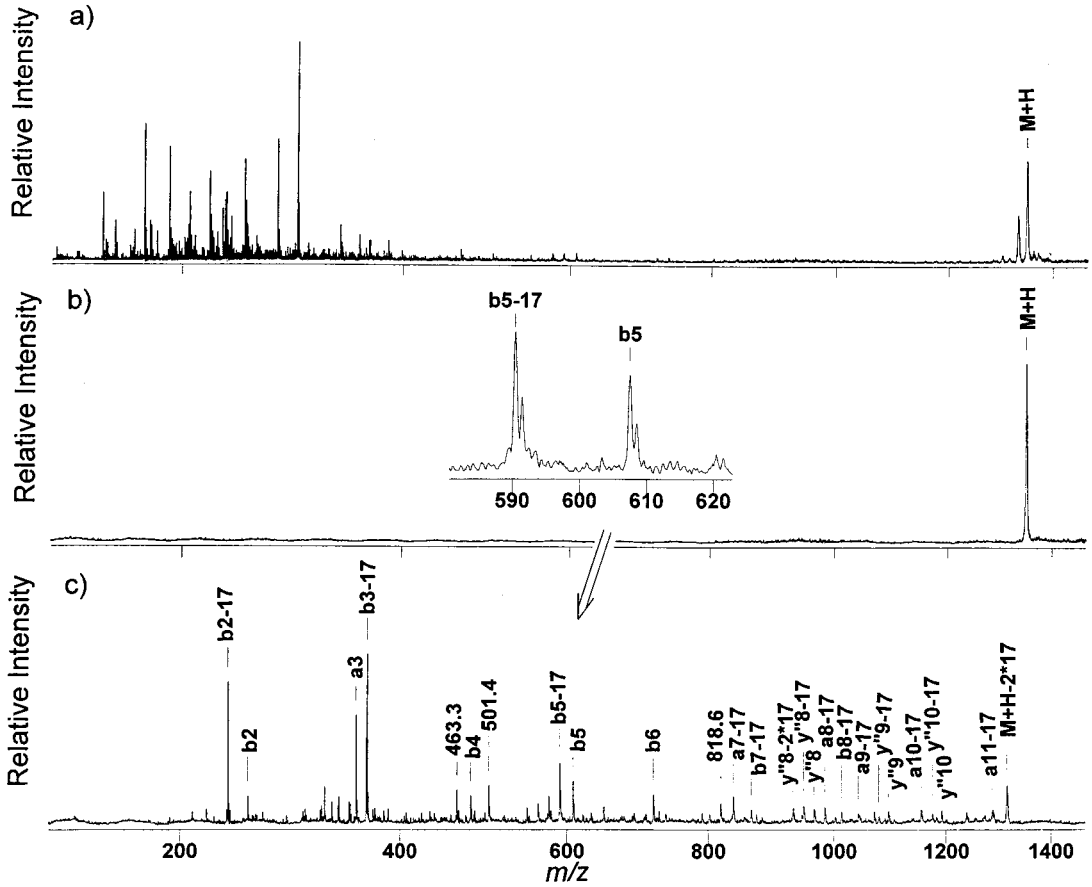

Figure 13. MALDI-QIT/reTOF mass spectra of substance P (M_r = 1347.7 Da): (a) after injection and storing for 50 ms; (b) after isolation of protonated molecules using a broadband excitation technique; (c) after fragmentation of the isolated ions via collisions with xenon molecules using a SORI excitation method.

case of symmetric bipolar extraction for two masses, m/z 200 and 500, are comparable to that reported in this work. The maximum mass resolution of 2000 achieved in the second study[51] for m/z 69–133 is close to that observed in this work. Also, the effect of the trapping r.f. field on the mass resolution was more pronounced for ions with the highest q_z values (lowest mass).

CONCLUSIONS

A MALDI-QIT/reTOF mass spectrometer was designed and tested in both normal and tandem (MS/MS) modes. The parabolic reflectron used in the instrument was capable of providing a theoretical mass resolution of 5000 for ions with a broad initial energy distribution spreading out over a 50% energy interval of the entire energy range of the reflectron. Modification of a standard commercial ion trap electrode geometry that included increasing the aperture for the extracted ions and stretching further the distance between the end-cap electrodes resulted in a good performance for a broadband excitation ion isolation method that is required for operation in the tandem mode. The sensitivity, ion isolation and CID efficiency in the MALDI-QIT/reTOF instrument were close to those observed in the MALDI/QIT mass spectrometer.[42]

The mass resolution of the MALDI-QIT/reTOF mass spectrometer was shown to depend on many parameters, including the extraction field potentials, the r.f. trapping voltage amplitude and the phase of shutting down the r.f. voltage before extraction. At low values of q_z (<0.3–0.4) the mass resolution behavior can be described in terms of the ion temperature, which was shown to be in the range 1180–1690 K. The mass resolution for all low-q_z ions is about the same and lies in the range 1000–1400 depending on the extraction voltages. The dependence of the mass resolution on the experimental parameters for ions at higher values of q_z (>0.4) is irregular but normally the mass resolution is lower than that for lower q_z ions. This irregular behavior is explained by the complex dependence of ion spatial and velocity distributions in the ion trap at high q_z values. A shift in mass spectral line positions was observed when the trapping voltage before extraction was varied. This shift is larger for low-mass (or high-q_z) ions and is comparable for these ions to the linewidths.

Acknowledgements

This work was supported in part by a grant from the National Institutes of Health (R01 RR08912) and was carried out at the Middle Atlantic Mass Spectrometry Laboratory.

REFERENCES

1. R. E. March and J. F. J. Todd (Eds), *Practical Aspects of Ion Trap Mass Spectrometry*, Vols 1, 2 and 3. CRC Press, Boca Raton, FL (1995).
2. G. C. Stafford, Jr, P. E. Kelley, J. E. P. Syka, W. E. Reynolds and J. F. J. Todd, *Int. J. Mass Spectrom. Ion Processes* **60**, 85 (1984).
3. M. G. Qian and D. M. Lubman, *Anal. Chem.* **67**, 234A (1995).
4. R. M. Waldren and J. F. J. Todd, *Int. J. Mass Spectrom. Ion Phys.* **29**, 315 (1979).
5. R. M. Waldren and J. F. J. Todd, *Int. J. Mass Spectrom. Ion Phys.* **29**, 337 (1979).
6. J. E Fulford and R. E. March, *Int. J. Mass Spectrom. Ion Phys.* **30**, 373 (1979).
7. R. M. Waldren and J. F. J. Todd, *Int. J. Mass Spectrom. Ion Phys.* **31**, 15 (1979).
8. E. R. Mosburg, M. Vedel, Y. Zerega, F. Vedel and J. Andre, *Int. J. Mass Spectrom. Ion Processes* **77**, 1 (1987).
9. R. J. Cotter, *Time-of-Flight Mass Spectrometry: Instrumentation and Applications in Biological Research.* ACS Professional Reference Books, Washington, DC (1997).
10. W. C. Wiley and I. H. McLaren, *Rev. Sci. Instrum.* **26**, 1150 (1955).
11. J. G. Boyle and C. M. Whitehouse, *Anal. Chem.* **64**, 2084 (1992).
12. O. A. Mirgorogskaya, A. A. Shevchenko, I. V. Chernushevich, A. F. Dodonov and A. I. Miroshnikov, *Anal. Chem.* **66**, 99 (1994).
13. A. N. Verentchikov, W. Ens and K. G. Standing, *Anal. Chem.* **66**, 126 (1994).
14. S. M. Michael, B. M. Chien and D. M. Lubman, *Rev. Sci. Instrum.* **63**, 4277 (1992).
15. S. M. Michael, B. M. Chien and D. M. Lubman, *Anal. Chem.* **65**, 2614 (1993).
16. B. M. Chien, S. M. Michael and D. M. Lubman, *Anal. Chem.* **65**, 1916(1993).
17. Th. L. Grebner and H. J. Neusser, *Int. J. Mass Spectrom. Ion Processes* **137**, L1 (1994).
18. Q. Ji, P. R. Vlasak, M. R. Davenport, C. G. Enke and J. F. Holland, *J. Am. Soc. Mass Spectrom.* **7**, 1009 (1996).
19. R. K. Julian and R. G. Cooks, *Anal. Chem.* **65**, 1827 (1993).
20. V. M. Doroshenko and R. J. Cotter, *Rapid Commun. Mass Spectrom.* **10**, 65 (1996).
21. G. Lawson and J. F. J. Todd, in *Dynamic Mass Spectrometry*, edited by D. Price and J. F. J. Todd, Vol. 4, p. 39. Heyden, London (1975).
22. K. P Aicher, M. Müller, U. Wilhelm and J. Grotemeyer, *Eur. Mass Spectrom.* **1**, 331 (1995).
23. P. Kofel, M. Stöckli, J. Krause and U. P. Schlunegger, *Rapid Commun. Mass Spectrom.* **10**, 658 (1996).
24. D. M. Chambers, S. W. Thomas, L. I. Grace and B. D. Andersen, in *Proceedings of the 43rd ASMS Conference on Mass Spectrometry and Allied Topics*, Atlanta, GA, 1995, p. 1138.
25. S. E. Buttrill and A. V. Mordehai, *US Pat.* 5569917 (1996).
26. R. B. Moore and M. D. Lunney, in *Practical Aspects of Ion Trap Mass Spectrometry*, edited by R. E. March and J. F. J. Todd, Vol. 2, p. 263. CRC Press, Boca Raton, FL (1995).
27. B. M. Chien, S. M. Michael and D. M. Lubman, *Rapid Commun. Mass Spectrom.* **7**, 837 (1993).
28. H. Lee and D. M. Lubman, *Anal. Chem.* **67**, 1400 (1995).
29. L. He, L. Liang and D. M. Lubman, *Anal. Chem.* **67**, 4127 (1995).
30. M. G. Qian, Y. Zhang and D. M. Lubman, *Rapid Commun. Mass Spectrom.* **9**, 1275 (1995).
31. B. M. Chien and D. M. Lubman, *Anal. Chem.* **66**, 1630 (1994).
32. U. Wilhelm, K. P Aicher and J. Grotemeyer, *Int. J. Mass Spectrom. Ion Processes* **152**, 111 (1996).
33. Y. Yoshida, *US Pat.* 4625112 (1986).
34. G. G. Managadze and I. Yu. Shutyaev, in *Laser Ionization Mass Spectrometry*; edited by A. Vertes, R. Gijbels and F. Adams, p. 505. Wiley, New York (1993).
35. C. A. Flory, R. C. Taber and G. E. Yefchak, *Int. J. Mass Spectrom. Ion Processes* **152**, 177 (1996).
36. P. Vlasak, D. J. Beussman, Q. Ji and C. G. Enke, *J. Am. Soc. Mass Spectrom.* **7**, 1002 (1996).
37. S. Guan and A. G. Marshall, *J. Am. Soc. Mass Spectrom.* **5**, 64 (1994).
38. B. D. Nourse and H. I. Kenttämaa, *J. Phys. Chem.* **94**, 5809 (1990).
39. C. Basic, J. R. Eyler and R. A. Yost, *J. Am. Soc. Mass Spectrom.* **3**, 716 (1992).
40. D. A. Dahl, *SIMION 3D Version 6.0 User's Manual.* Princeton Electronic Systems, Princeton, NJ (1995).
41. A. A. Makarov, E. N. Raptakis and P. J. Derrick, *Int. J. Mass Spectrom. Ion Processes* **146**, 165 (1995).
42. V. M. Doroshenko and R. J. Cotter, *Anal. Chem.* **68**, 463 (1996).
43. V. M. Doroshenko and R. J. Cotter, *J. Mass Spectrom.* **31**, 602 (1997).
44. V. M. Doroshenko and R. J. Cotter, *Rapid Commun. Mass Spectrom.* **7**, 822 (1993).
45. V. M. Doroshenko and R. J. Cotter, *Rapid Commun. Mass Spectrom.* **8**, 766 (1994).
46. V. M. Doroshenko and R. J. Cotter, *Rapid Commun. Mass Spectrom.* **10**, 1921 (1996).
47. J. W. Gauthier, T. R. Trautman and D. B. Jocobson, *Anal. Chim. Acta* **246**, 211 (1991).
48. I. A. Kaltashov, V. M. Doroshenko and R. J. Cotter, *Proteins: Struct. Funct. Genet.* **28**, 53 (1997).
49. U. Wilhelm, C. Weickhardt and J. Grotemeyer, *Rapid Commun. Mass Spectrom.* **10**, 473 (1996).
50. L. He and D. M. Lubman, *Rapid Commun. Mass Spectrom.* **11**, 1467 (1997).
51. D. M. Chambers, L. I. Grace and B. D. Andersen, *Anal. Chem.* **69**, 3780 (1997).